Ray-tracing critical-angle transmission gratings for the X-ray Surveyor and Explorer-size missions

Hans M. Günther, Marshall W. Bautz, Ralf K. Heilmann, David P. Huenemoerder, Herman L. Marshall, Michael A. Nowak, and Norbert S. Schulz

Massachusetts Institute of Technology, MIT Kavli Institute for Astrophysics and Space Research, 77 Massachusetts Avenue, Cambridge, MA 02139

ABSTRACT

We study a critical angle transmission (CAT) grating spectrograph that delivers a spectral resolution significantly above any X-ray spectrograph ever flown. This new technology will allow us to resolve kinematic components in absorption and emission lines of galactic and extragalactic matter down to unprecedented dispersion levels. We perform ray-trace simulations to characterize the performance of the spectrograph in the context of an X-ray Surveyor or Arcus like layout (two mission concepts currently under study).

Our newly developed ray-trace code is a tool suite to simulate the performance of X-ray observatories. The simulator code is written in Python, because the use of a high-level scripting language allows modifications of the simulated instrument design in very few lines of code. This is especially important in the early phase of mission development, when the performances of different configurations are contrasted. To reduce the run-time and allow for simulations of a few million photons in a few minutes on a desktop computer, the simulator code uses tabulated input (from theoretical models or laboratory measurements of samples) for grating efficiencies and mirror reflectivities.

We find that the grating facet alignment tolerances to maintain at least 90% of resolving power that the spectrometer has with perfect alignment are (i) translation parallel to the optical axis below 0.5 mm, (ii) rotation around the optical axis or the groove direction below a few arcminutes, and (iii) constancy of the grating period to 1:10^5. Translations along and rotations around the remaining axes can be significantly larger than this without impacting the performance.

Keywords: ray-tracing, X-ray optics, critical angle transmission grating, X-ray Surveyor, Arcus

1. INTRODUCTION

The availability of the X-ray grating spectrometers on Chandra and XMM-Newton has opened an enormous discovery space in X-ray astronomy. The resolving power of the gratings on these satellites is roughly an order of magnitude higher than that of their imaging CCD detectors. In the soft X-rays (about 1-10 nm) only grating spectroscopy can resolve individual lines in the coronae of cool stars (where certain line ratios provide a temperature and density diagnostic), resolve line profiles in kinematically broadened lines formed in the radiation powered winds of hot stars, measure individual abundances in planetary nebulae, and detect absorption edges in the interstellar medium (ISM), to give just a few examples. In many cases, the insight gained from X-ray grating spectroscopy is unique, because no other bandpass contains detailed diagnostics for highly ionized plasmas. For wavelength below 1 nm microcalorimeters reach a spectral resolution comparable to grating spectroscopy.

X-ray grating spectroscopy currently requires long exposure times on relatively bright targets, because of the small effective area of Chandra and XMM-Newton and the low efficiency of their gratings. To move forward, we need instruments with a much larger collecting area and gratings that transmit a larger fraction of the photons, preferably into high diffraction orders to further increase the spectral resolution. Such new technology will allow us to resolve kinematic components in absorption and emission lines of galactic and extra-galactic matter down to unprecedented resolution.

Send correspondence to H.M.G.
E-mail: hgunther@mit.edu

Space Telescopes and Instrumentation 2016: Ultraviolet to Gamma Ray, edited by Jan-Willem A. den Herder, Tadayuki Takahashi, Marshall Bautz, Proc. of SPIE Vol. 9905, 990556 · © 2016 SPIE · CCC code: 0277-786X/16/$18 · doi: 10.1117/12.2232157

In this work, we study a spectrometer based on critical angle transmission (CAT) gratings (see Ref. 1 for operating principles of CAT gratings). In brief, CAT gratings are blazed transmission gratings. They combine the advantages of traditional transmission gratings (relaxed alignment tolerances, low mass, low temperature sensitivity, transparency at high energies) and blazed reflection gratings (high diffraction efficiency, blazing into high diffraction orders for high spectral resolution). Blazing is achieved by tilting the gratings by a blaze angle below the critical angle for total external reflection, such that x-rays are efficiently reflected off the grating bar sidewalls.

The performance of a spectrometer depends critically on the design parameters of other mission components. For example, a mirror with a well-focused point-spread function (PSF) allows for higher spectral resolution with otherwise identical grating parameters, so we study optics proposed for two recent missions, the X-ray Surveyor[2] and Arcus.[3] In both cases, the mission parameters are still under development, and we do not intend to reproduce the exact specifications that are given in other presentations in this volume; rather, we intend to determine what spectral resolution is achievable with CAT gratings and whether such an instrument can reasonably meet or exceed the minimum requirements of these missions. The X-ray Different mirror technologies are being considered for the X-ray Surveyor and Arcus missions (see Sect. 3), so it is interesting to contrast the expected grating performance for both.

The organization of this paper is as follows: In Sect. 2 we describe our ray-tracing code. In Sect. 3 we describe the setup that we use to represent the X-ray Surveyor and Arcus. Section 4 contains our results, which we discuss in Sect. 5.

2. RAY-TRACING CODE

MARXS (Multi-Architecture-Raytrace-Xraymission-Simulator) is a tool suite to simulate the performance of X-ray observatories. It is primarily aimed at astronomical X-ray satellites and sounding rocket payloads, but can be used to ray-trace experiments in the laboratory as well. MARXS performs Monte-Carlo ray-trace simulations from a source (astronomical or lab) through a collection of optical elements such as mirrors, baffles, and gratings to a detector.

The design of MARXS is optimized with the following principles and ideas in mind:

Flexibility In the design and proposal phase of a mission many different science goals will be simulated for different satellite geometries and different instrument configurations. MARXS shall make it easy to simulate arbitrary combinations of optical elements in very few lines of code.

Generality MARXS shall provide classes that cover all the common elements in X-ray instruments e.g. Wolter Type I mirrors, baffles, gratings, multi-layer mirrors, detectors. The classes can be extended for special use cases not covered by MARXS modules.

Simplicity MARXS was designed to solve the ray-trace problem in a simple prescription, e.g., it solves the grating equation, but requires an input table to select the grating order for each photon because solving Maxwell's equations to calculate these probabilities is a complex and computationally expensive problem.

Developer time is more valuable than CPU time. MARXS shall be fast enough to run on a desktop PC for a reasonable number of photons (a million photons can be ray-traced in a few minutes), but the flexibility of the code is more important than speed optimization.

Order of optical elements is known. MARXS assumes that the order in which photons hit (or miss) optical elements is known in advance, e.g., entrance aperture to mirror to grating to detector.

MARXS is written in Python, making use of several well-established packages for numerics and scientific computations (numpy and scipy,[4] and astropy[5]). It is available under the GPL3 license at `https://github.com/chandra-marx/marxs`, but at this time the code is still under development and no stable version has been released. MARXS makes heavy use of unit tests to verify individual modules by comparison with analytic results.

The default coordinate system in MARXS places the origin at the mirror focus. The mirror optical axis coincides with the x-axis of the coordinate system and astrophysical sources are located at $x = +\infty$. Aligned gratings disperse the spectrum along the y-axis, thus the cross-dispersion axis falls along the z-axis.

3. MISSION LAYOUT

The performance of any grating spectrometer depends critically on the size of the PSF that the mirror delivers and on the distances between the gratings and the detectors, which are typically similar to the focal length of the mirror. We present simulations for two setups, which resemble two recently proposed X-ray missions. In both cases, the design parameters are not finalized and might differ from the numbers we assume here.

The two important performance metrics for a spectrometer are its resolving power and its effective area. In this work, we concentrate on the resolving power; thus, we simulate the geometry of the mirrors, but not their correct effective area. All our simulations are for on-axis sources because off-axis sources are only rarely observed with gratings: The PSF is wider and parts of the dispersed spectrum will not fall on the detectors, which are designed for on-axis sources. Thus, the mirror modules used for our simulations do not need to have the same off-axis performance as the mirror systems proposed for the X-ray Surveyor or Arcus.

3.1 X-ray Surveyor

The X-ray Surveyor mission concept calls for a mirror with a large effective area and less than half-arcsecond angular resolution. Current plans for the mirror forsee a Wolter-Schwarzschild design that has a good on-axis performance, but does not degrade as fast as the PSF from a Wolter Type I mirror for larger off-axis angles.[2] While the X-ray Surveyor might have several detectors including a microcalorimeter, the grating spectrum will be read-out with a CMOS or CCD with pixels so small that the pixel size does not degrade the spectrometer resolving power significantly. In the simulation we assume detectors with arbitrarily small pixels.

For our simulation, we use the Wolter Type I Chandra mirror as implemented in MARX.[6] It provides a PSF below 0.5 arcseconds FWHM in the focal point. We use a focal length of 9 m for our calculations. Grating facets are placed behind all four mirror shells in a single wedge with an azimutal range of 30°. In this configuration, only 12 60×60 mm^2 grating facets are required.

3.2 Arcus

Arcus was originally proposed as an instrument mounted on the International Space Station,[3] but is now re-designed as a NASA explorer mission (see paper 9905-218 in this volume). It will reuse silicon pore optics (SPO) designed for the ESA Athena mission[7,8] and inherits Athena's 12 m focal length. The current design calls for off-plane diffraction gratings, but in this work we show that CAT gratings are a viable alternative. Arcus will fly with CCD detectors, again with pixels small enough that they do not significantly impact the resolving power of the spectrometer and in the simulation we assume detectors with arbitrarily small pixels.

For our simulation, we use a mirror that perfectly focuses all rays and then add an extra Gaussian blur in the in-plane and off-plane directions to reproduce the bow-tie shaped PSF (which is due to filling only a small azimuthal range of the aperture) seen in Ref. 9. We use a Gaussian with $\sigma = 3.4$ arcsec (i.e. $FWHM = 8.2$ arcsec) for in-plane scatter and 0.4 arcsec for off-plane scatter; these number are estimated from the measured performance of a single mirror module shown in Ref. 10 (their Fig. 2).

The placement of the grating facets for the Arcus simulation is sketched in Fig. 1 (not to scale). The opening aperture has the shape of a single wedge with an azimutal range of 30°. Grating facets are placed in dense rings to fill most of the available space without overlapping two facets. In the configuration we simulate, 25 20×20 mm^2 facets are required for Arcus.

3.3 CAT grating spectrometer

For the X-ray Surveyor study we place CAT gratings on a ring just below the mirror shells, where the radius of the ring matches the radius of the corresponding mirror shell, similar to the design in the Chandra/HETG,[11] but we use sub-aperturing, where gratings only fill a small wedge with an azimutal range of 30°. For an Arcus-like design with SPO optics consisting of a large number of shells, we fill a wedge with the same opening angle with gratings, leaving a few mm of space between them to allow for mounting on a structure. In both cases, grating efficiencies are read in from pre-calculated tables. The efficiency tables are based on rigorous coupled-wave analysis (RCWA) simulations for silicon CAT gratings with 200 nm period, using commercial software (GSolver) or custom code.[12] For the X-ray Surveyor tables we modeled 6.1 micron deep and 40 nm wide grating bars,

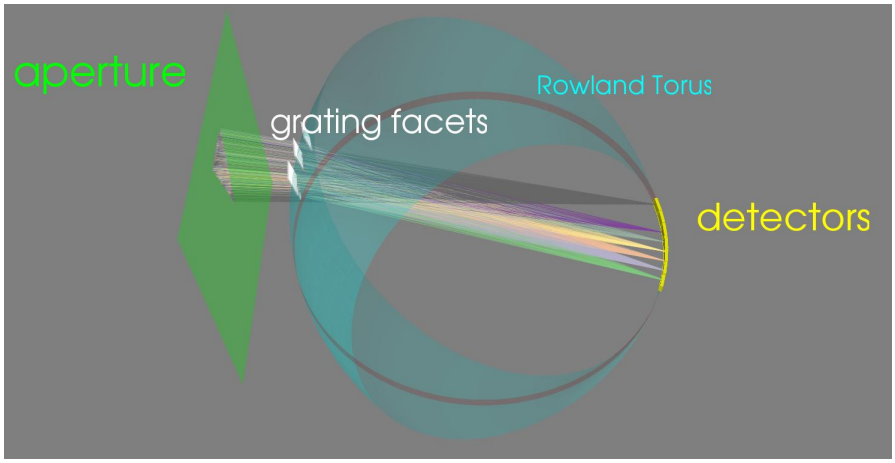

Figure 1. Rendering of the layout of the spectrograph (not to scale). Photons enter through a wedge-shaped hole in the aperture plane (green). Individual grating facets (white) are located in the path of the rays. They are inclined towards the Rowland torus (blue). Detectors (yellow) are placed in the Rowland circle to cover the zeroth order and higher orders. In this example, all photons have the same wavelength and they are refracted into orders 3 to 8. Individual rays are color coded by the diffraction order that they are diffracted into, where gray is the zeroth order.

while the Arcus tables assume 4.0 micron deep gratings with 60 nm wide bars. CAT gratings with the latter dimensions have been routinely produced with 250 mm^2 area[1] and we expect the former to be available in time for the X-ray Surveyor mission. The modeled grating facets are square with 20 mm on each side for Arcus and 60 mm for the X-ray Surveyor.

Individual grating facets are placed on a Rowland torus,[13] and oriented such that the angle between the grating normal and a ray going through the center of the facet towards the focal point is the blaze angle, which is 1.5° for the X-ray surveyor gratings and 1.9° for Arcus. The Rowland torus is tilted by twice the blaze angle with respect to the optical axis as in Ref. 14. This geometry reduces the distance between the edges of the facets and the Rowland torus compared to a geometry where the center of the Rowland circle falls onto the optical axis. A rendering of the geometry is shown in Fig. 1.

The simulations include the effect of the finite size of the facets. Since facets are flat, they cannot match the Rowland torus at all points. This effect is negligible for small facets, but might impact resolving power in the simulations for the X-ray Surveyor.

4. RESULTS

In this section we present results for our ray-trace calculations for the two different setups.

4.1 Resolving power

Figure 2 shows a zoom into a sample of images on the detector for monochromatic simulations with photons of wavelength 1.24 nm. We show the mirror PSF in the zeroth order and the diffraction order that receives the largest number of photons at this wavelength for both of our scenarios. The PSF for the X-ray Surveyor is much narrower than Arcus, where a few photons is scattered far into the wings. The Arcus PSF has the bow-tie shape discussed above.

We fit a Gaussian to the distribution of the photons in the dispersion direction, read-off the full width at half-maximum (FWHM), and define the resolving power as:

$$R = \frac{\lambda}{\Delta\lambda} = \frac{d_x}{FWMH} \tag{1}$$

where λ is the wavelength of a spectral line with negligible intrinsic width, and $\Delta\lambda$ is the observed width of this feature. Since the detector does not give the wavelength directly, d_x and the $FWHM$ are linear distances

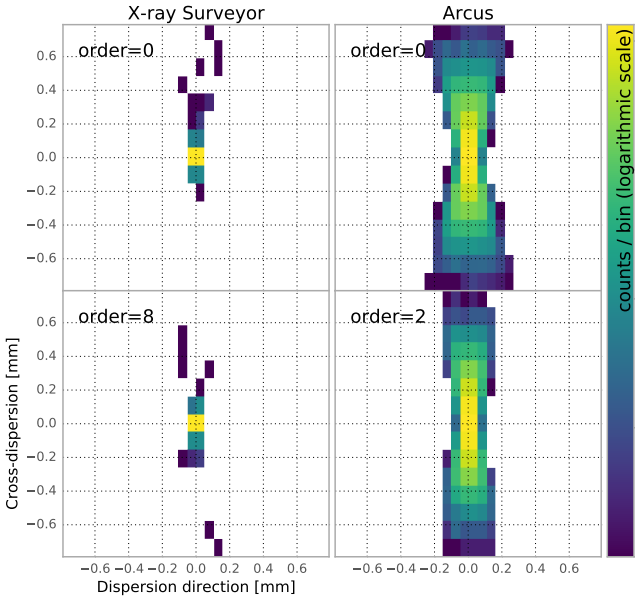

Figure 2. Distribution of 1.24 nm photons on the detector in the zeroth order (not diffracted) and in the order that receives the largest number of diffracted 1.24 nm photons, which is the 8th order for the X-ray Surveyor and the 2nd order for Arcus. For each subplot, the coordinate system is centered on the peak of the distribution to make it easy to compare the scales. (The assumed blaze angle of 1.9 deg for Arcus is greater than the critical angle for 1.24 nm x-rays on silicon, i.e. blazing is weak and smaller orders are stronger.) Photons are binned for display purposes.

measured along a curved detector that follows the Rowland circle. The $FWMH$ is the full width at half maximum of the event distribution and d_x is the distance between the center of a diffracted order and the zeroth order. The resolving power for 1.24 nm photons in order 8 is about 20000. Simulations of this type are repeated for a range of wavelengths and for diffraction orders from 1 to 10. Figure 3 shows the measured resolving power. In each case, we run the simulation long enough to collect 10^4 photons in every order. For long wavelengths the resolving power drops for high orders because the diffraction angles become large (up to 30°) and effects where the flat, finite grating facet deviates from the ideal Rowland torus become important. However, in practice these orders are not relevant, because the grating efficiencies for long wavelengths are very low for such high grating orders. At least for Arcus, most photons with $\lambda > 4$ nm are diffracted into order 1 or 2.

Scientific goals depend on both resolution and efficiency, thus we define an efficiency weighted resolving power, where the effective resolving power is calculated for individual orders as described above and then weighted with the diffraction efficiency for that particular order. This number is shown in Fig. 4.

4.2 Misalignments

The optimal resolving power requires that grating facets and detectors are located exactly on the Rowland torus. We repeat the simulations, adding a random misalignment to each grating facet, which is drawn from a Gaussian distribution. This misalignment can be a linear translation (Fig. 5) or a rotation (Fig. 6). For a larger number of facets, the drawn distribution will be close to Gaussian and one would expect smooth curves in the resulting plots. However, our models have only 12 and 25 facets respectively, so some scatter can be seen in the figures.

Figure 5 shows how the resolving power decreases when grating facets are displaced. Moving facets parallel to the optical axis quickly degrades the resolving power. A misalignment of 0.5 mm reduces the resolving power for long wavelength by one third in the Arcus case. In contrast, tolerances are much larger perpendicular to the optical axis, because this is essentially along the surface of the Rowland torus.

Figure 6 shows the analogous plot for rotational misalignments. Again, the tolerances along the different axes are vastly different. Rotation about the z-axis (the cross-dispersion direction on the detector) is the most

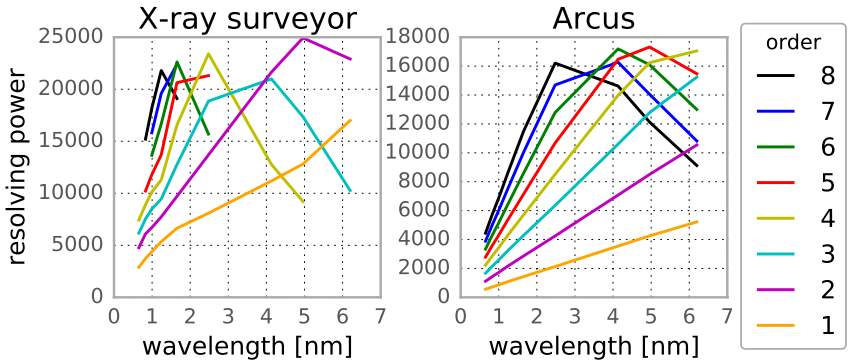

Figure 3. Resolving power at different wavelengths for different orders.

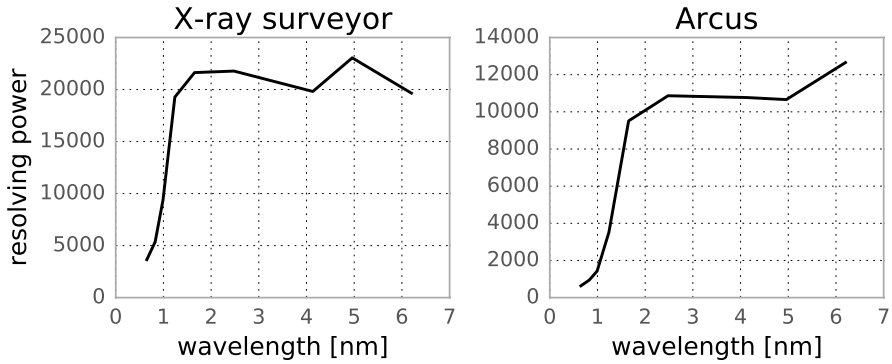

Figure 4. Efficiency weighted resolving power. Both missions have consistently high resolving power above 2 nm.

severe problem because this reduces the effective grating constant as seen by the photons (projected into a plane normal to the direction of photon propagation). Thus, photons are dispersed more or less, which widens the image of the grating order. Rotations around the optical axis are less severe and rotation around the grating dispersion direction does not influence the resolving power even if the misalignment reaches 1 degree.

4.3 Variability of the grating period

If the grating period of the CAT gratings is not uniform within a grating or differs between gratings, the resolving power of the system as a whole will decrease because some photons are diffracted more or less than those that pass through gratings with the nominal grating period of 200 nm. Figure 7 assumes that the deviations from the nominal value can be described by a normal distribution. Curves for all wavelengths follow a very similar shape, but the drop of the resolving power starts for slightly smaller relative errors for large wavelengths. To retain optimal resolution, the relative period error in the facet period should be kept below $1:10^5$. Chandra gold bar HETGs, supported by pliable polyimide membranes, were already fabricated with periods constant to $1:4\times10^4$ a generation ago.[11] Progress in patterning[15] and fabrication techniques put $1:10^5$ for CAT gratings made from much stronger silicon well in reach. Experimentally $R > 10,000$ has already been demonstrated at 0.83 nm wavelength with CAT gratings.[16]

5. DISCUSSION

We present ray-trace simulations for two currently discussed mission concepts (the X-ray Surveyor and Arcus) and show the spectral resolving power that can be achieved with CAT gratings in the context of these missions. We find a resolving power around 20000 for 2-6 nm photons for the X-ray Surveyor and around 10000 for Arcus in the same wavelength range. This difference is mostly due to the much sharper PSF that we used for the

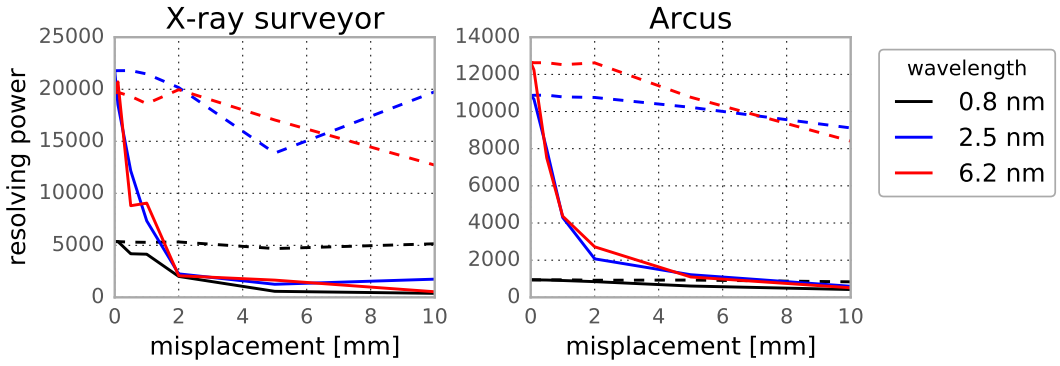

Figure 5. Degradation of resolving power due to misalignment along the optical axis (solid lines) or perpendicular to it (dashed lines). The x-axis shows the standard deviation of the grating facets from the ideal prescription; the y-axis shows the resolving power averaged over all observable orders.

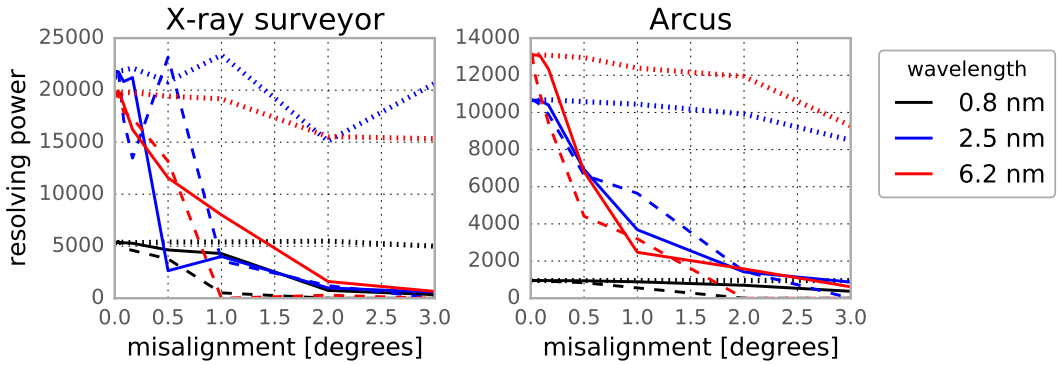

Figure 6. Same as Fig. 5, but for rotation around the optical axis (solid lines), the dispersion direction (dotted lines), and cross-dispersion direction (dashed lines).

X-ray Surveyor simulations; however there are several factors that limit the resolving power even in the X-ray Surveyor case. The X-ray Surveyor simulation assumes facet sizes of 60 mm. Their center position is placed on the Rowland Torus and they are rotated to match the expected blaze angle. This means that (i) some rays are intersected away from the surface of the Rowland torus, which causes mostly a lateral offset in where the ray lands on the detector and (ii) rays hitting the edges of the facets will have a blaze angle (since the rays converge to the focal point and are not parallel) that differs from the expected one by up to 0.15 degrees, which causes a change in the diffraction efficiency, but also a small difference in the diffraction angle. In principle this effect can be ameliorated to a large degree by adding a weak chirp to the grating period. These effects of a finite facet size are a lot smaller for Arcus, simply because the facets are only 20 mm on each side. Also, for Arcus we assumed gratings with a larger blaze angle and a longer focal length, both leading to a higher resolving power and partially compensating for the larger PSF when compared to the X-ray Surveyor simulations.

We performed a series of simulations to quantify the impact of different types of misalignment; they are summarized in table 1. The spectral resolving power in the wavelength range of interest degrades by more than 10% for a linear displacement of the facets parallel to the optical axis above about 0.5 mm, while displacement perpendicular to the optical axis of several mm has no measurable impact. Similarly, a rotation around the dispersion axis (perpendicular to the groove direction of the grating facets) can be several degrees, while rotations around the optical axis and around an axis parallel to the groove direction degrade the resolving power by more then 10% if they exceed a few arcminutes which are very comfortable tolerances. Last, the grating period has to be stable to about $1{:}10^5$.

As can be seen on the figures, the limits that our simulations set for alignment uncertainties and period facet

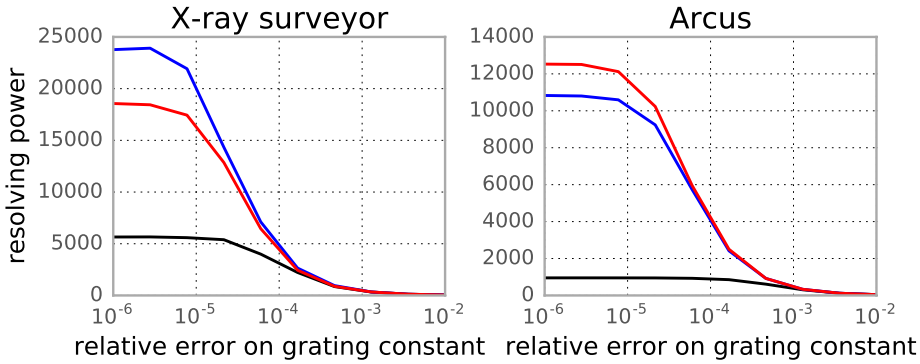

Figure 7. Degradation of the resolving power due to variability in the grating period for different wavelengths (see Fig. 5 for color code). *left:* X-ray Surveyor; *right:* Arcus.

Table 1. Tolerances for facet misalignments to keep the spectral resolving power within 10% of the maximum.

Error source	value
Translation parallel to optical axis	0.5 mm
Translation perpendicular to optical axis	5 mm
Rotation around optical axis	5 arcmin
Rotation around groove direction	5 arcmin
Rotation perpendicular to grooves and optical axes	5 degrees
Stability of grating period	$1{:}10^5$

variations are very similar for different wavelengths and for the X-ray Surveyor and the Arcus scenario, which use different focal lengths (9 m and 12 m, respectively), different mirror types (a few well-controlled shells and hundreds of thin shells in the silicon pore-optics) with different point-spread functions, and a different geometry for the placement of the grating facets (on rings under the mirror shells and space-filling). While the absolute numbers for the spectral resolving power will change significantly as the mirror specifications of both concepts evolve, we expect the putative alignment tolerances to be relatively robust.

In this proceeding we concentrated on the discussion of the spectral resolving power, but we can also derive the effective area from our simulations. Like the resolving power, the absolute number depends on the parameters of the mirror. If the support structure that holds the individual grating facets can be designed to be placed in those regions that are already shaded by mirror support struts, then CAT gratings can fill most of the available area. Efficiencies for individual gratings are discussed in Ref. 1.

Ref. 9 performs a detailed analytic and numerical study of off-plane grating (OPG) performance and alignment tolerances. While not directly comparable to our scenarios, their setup is similar enough that we can compare the order of magnitude of the alignment tolerances. For OPGs this is of order a few arcseconds for rotations and a few hundred micron for translations in two spatial directions. In contrast, CAT gratings are far more forgiving with rotational tolerances of arcminutes and only one translational direction has to be kept below 0.5 mm.

ACKNOWLEDGMENTS

Support for this work was provided by NASA through the Smithsonian Astrophysical Observatory (SAO) contract SV3-73016 to MIT for Support of the Chandra X-Ray Center (CXC) and Science Instruments. CXC is operated by SAO for and on behalf of NASA under contract NAS8-03060.

REFERENCES

[1] Heilmann, R. K., Bruccoleri, A. R., and Schattenburg, M. L., "High-efficiency blazed transmission gratings for high-resolution soft x-ray spectroscopy," *Proc. SPIE* **9603**, 960314–960314–12 (2015).

[2] Gaskin, J. A., Weisskopf, M. C., Vikhlinin, A., Tananbaum, H. D., Bandler, S. R., Bautz, M. W., Burrows, D. N., Falcone, A. D., Harrison, F. A., Heilmann, R. K., Heinz, S., Hopkins, R. C., Kilbourne, C. A., Kouveliotou, C., Kraft, R. P., Kravtsov, A. V., McEntaffer, R. L., Natarajan, P., ODell, S. L., Petre, R., Prieskorn, Z. R., Ptak, A. F., Ramsey, B. D., Reid, P. B., Schnell, A. R., Schwartz, D. A., and Townsley, L. K., "The x-ray surveyor mission: a concept study," *Proc. SPIE* **9601**, 96010J–96010J–14 (2015).

[3] Smith, R. K., Ackermann, M., Allured, R., Bautz, M. W., Bregman, J., Bookbinder, J., Burrows, D., Brenneman, L., Brickhouse, N., Cheimets, P., Carrier, A., Freeman, M., Kaastra, J., McEntaffer, R., Miller, J., Ptak, A., Petre, R., and Vacanti, G., "Arcus: an iss-attached high-resolution x-ray grating spectrometer," *Proc. SPIE* **9144**, 91444Y–91444Y–12 (2014).

[4] Jones, E., Oliphant, T., Peterson, P., et al., "SciPy: Open source scientific tools for Python," (2001–). [Online; accessed 2016-06-04].

[5] Astropy Collaboration, Robitaille, T. P., Tollerud, E. J., Greenfield, P., Droettboom, M., Bray, E., Aldcroft, T., Davis, M., Ginsburg, A., Price-Whelan, A. M., Kerzendorf, W. E., Conley, A., Crighton, N., Barbary, K., Muna, D., Ferguson, H., Grollier, F., Parikh, M. M., Nair, P. H., Unther, H. M., Deil, C., Woillez, J., Conseil, S., Kramer, R., Turner, J. E. H., Singer, L., Fox, R., Weaver, B. A., Zabalza, V., Edwards, Z. I., Azalee Bostroem, K., Burke, D. J., Casey, A. R., Crawford, S. M., Dencheva, N., Ely, J., Jenness, T., Labrie, K., Lim, P. L., Pierfederici, F., Pontzen, A., Ptak, A., Refsdal, B., Servillat, M., and Streicher, O., "Astropy: A community Python package for astronomy," *A&A* **558**, A33 (Oct. 2013).

[6] Wise, M. W., Huenemoerder, D. P., and Davis, J. E., "Simulated {AXAF} Observations with {MARX}," in [*Astronomical Data Analysis Software and Systems VI*], G. Hunt & H. Payne, ed., *Astronomical Society of the Pacific Conference Series* **125**, 477 (1997).

[7] Willingale, R., Pareschi, G., Christensen, F., den Herder, J.-W., Ferreira, D., Jakobsen, A., Ackermann, M., Collon, M., and Bavdaz, M., "Science requirements and optimization of the silicon pore optics design for the athena mirror," *Proc. SPIE* **9144**, 91442E–91442E–9 (2014).

[8] Collon, M. J., Vacanti, G., Gnther, R., Yanson, A., Barrire, N., Landgraf, B., Vervest, M., Chatbi, A., Beijersbergen, M. W., Bavdaz, M., Wille, E., Haneveld, J., Koelewijn, A., Leenstra, A., Wijnperle, M., van Baren, C., Mller, P., Krumrey, M., Burwitz, V., Pareschi, G., Conconi, P., and Christensen, F. E., "Silicon pore optics development for athena," *Proc. SPIE* **9603**, 96030K–96030K–11 (2015).

[9] Allured, R. and McEntaffer, R. T., "Analytical alignment tolerances for off-plane reflection grating spectroscopy," *Experimental Astronomy* **36**, 661–677 (Dec. 2013).

[10] Collon, M. J., Ackermann, M., Günther, R., Chatbi, A., Vacanti, G., Vervest, M., Yanson, A., Beijersbergen, M. W., Bavdaz, M., Wille, E., Haneveld, J., Olde Riekerink, M., Koelewijn, A., van Baren, C., Müller, P., Krumrey, M., Burwitz, V., Sironi, G., and Ghigo, M., "Making the athena optics using silicon pore optics," *Proc. SPIE* **9144**, 91442G–91442G–8 (2014).

[11] Canizares, C. R., Davis, J. E., Dewey, D., Flanagan, K. A., Galton, E. B., Huenemoerder, D. P., Ishibashi, K., Markert, T. H., Marshall, H. L., McGuirk, M., Schattenburg, M. L., Schulz, N. S., Smith, H. I., and Wise, M., "The Chandra High-Energy Transmission Grating: Design, Fabrication, Ground Calibration, and 5 Years in Flight," *PASP* **117**, 1144–1171 (Oct. 2005).

[12] Heilmann, R. K., Ahn, M., Bruccoleri, A., Chang, C.-H., Gullikson, E. M., Mukherjee, P., and Schattenburg, M. L., "Diffraction efficiency of 200-nm-period critical-angle transmission gratings in the soft x-ray and extreme ultraviolet wavelength bands," *Appl. Opt.* **50**, 1364–1373 (Apr 2011).

[13] Paerels, F., "X-ray Diffraction Gratings for Astrophysics," *Space Sci. Rev.* **157**, 15–24 (Dec. 2010).

[14] Heilmann, R. K., Davis, J. E., Dewey, D., Bautz, M. W., Foster, R., Bruccoleri, A., Mukherjee, P., Robinson, D., Huenemoerder, D. P., Marshall, H. L., Schattenburg, M. L., Schulz, N. S., Guo, L. J., Kaplan, A. F., and Schweikart, R. B., "Critical-angle transmission grating spectrometer for high-resolution soft x-ray spectroscopy on the international x-ray observatory," *Proc. SPIE* **7732**, 77321J–77321J–11 (2010).

[15] Heilmann, R. K., Chen, C. G., Konkola, P. T., and Schattenburg, M. L., "Dimensional metrology for nanometre-scale science and engineering: towards sub-nanometre accurate encoders," *Nanotechnology* **15**(10), S504 (2004).

[16] Heilmann, R. K., Bruccoleri, R. K., Kolodziejczak, A., Gaskin, J., O'Dell, S. L., Bathia, R., and Schattenburg, M. L., "Critical-angle x-ray transmission grating spectrometer with extended bandpass and resolving power > 10,000," *Proc. SPIE* **this volume**, 9905–65.